

Enhanced Single-Photon Detector: Achieving Superconducting-Level Performance with Conventional Quantum Technology

Hao Shu^{1*}

^{1*}Sun Yat-Sen University, Guangzhou, 510000, Guangdong, China.

Corresponding author(s). E-mail(s): Hao_B_Shu@163.com;

Abstract

High-performance single-photon detectors (SPDs) are indispensable components for quantum optical tasks. However, the reliance of state-of-the-art devices on superconducting materials imposes severe technological demands and challenging operational conditions (e.g., cryogenics), which hinder scalable commercial deployment. To address this, we propose the Enhanced Single-Photon Detector (ESPD) framework, a novel paradigm for achieving high-performance SPDs through the iterative enhancement of low-technology SPDs. Utilizing only standard quantum optical components, the ESPD scheme transforms a legacy non-superconducting SPD, with detection efficiency (DE) about **59%** and dark count rate (DCR) 10^{-2} , into a device with superior performance metrics, achieving DE higher than **95%** and DCR below 10^{-9} . This level of performance is comparable to or surpasses recently designed superconducting SPDs, allowing the minimal tolerable channel transmission rate for Quantum Key Distribution (QKD) protocols to be reduced by several orders of magnitude. Furthermore, the scheme's device requirements are moderate, relying on readily available current technology, which ensures near-term experimental feasibility. The ESPD framework thus provides a clear, scalable path toward the large-scale deployment of high-performance SPDs and the commercialization of quantum communication technologies.

Keywords: Single photon-detector, Detective efficiency, Dark count rate, Quantum optics, Quantum key distribution

1 Introduction

Single-photon detectors (SPDs) play a pivotal role in quantum optics, as measurement is indispensable for information readout across virtually all applications. The two most critical performance metrics of an SPD are the detection efficiency (DE), denoted by η , and the dark count rate (DCR), denoted by d . The former influences the efficiency of nearly all quantum operations, while the latter constitutes the ultimate limitation in high-attenuation scenarios. Regarding DE, numerous quantum experiments rely on SPD signals to retrieve results. In linear optical quantum computation, where success events are probabilistic and require the simultaneous detection of multiple photons, the success rate decreases exponentially with low-efficiency SPDs [1–3]. In Bell tests for quantum non-locality, verifying violations of the Clauser–Horne–Shimony–Holt or Eberhard inequalities routinely requires DE exceeding specific thresholds to close loopholes [4–10], such as approximately 67% [11] or 83% [12]. In heralded single-photon sources, where entangled pairs are generated and one photon is detected to confirm the presence of the other, the efficiency of the SPD directly dictates the success rate [13–16]. Regarding DCR, a primary constraint arises in quantum communication, particularly in quantum key distribution (QKD). The security of a practical QKD protocol relies on maintaining the quantum bit error rate (QBER) below a protocol-specific threshold, which is significantly lower than 50% [17–20]. However, communication channels induce exponential photon attenuation [21–24]. If the effective signal rate, determined by the channel transmission rate and thus communication distance, falls below the DCR of the SPDs, the QBER rises precipitously, as dark count events (which yield a 50% error rate) dominate the detection statistics. Consequently, the practical secure distance of QKD is strictly limited by the DCR of the SPDs [25–27].

Given their critical importance, the development of SPDs has been a continuous research focus since the inception of quantum technologies. While capable of operating at room temperature, traditional SPDs often suffer from both low DE and high DCR. For instance, a frequency upconversion SPD presented in 2004 operates at 300 K with a DE of approximately 59% and a DCR of 10^{-2} [28], while an InGaAs/InP detector presented in 2017 operates at 223 K with a DE of 27.5% and a DCR of 10^{-6} [29]. These specifications are insufficient for advanced quantum tasks, which typically require the DE of SPD above 90% with DCR below 10^{-7} . To suppress DCR and enhance DE, recent efforts have shifted toward designing SPDs using superconducting devices, such as superconducting nanowire SPDs (SNSPDs) [30–33]. These detectors achieve performance superior to traditional counterparts, boosting DE to over 90% while suppressing DCR by several orders of magnitude. This capability enables the implementation of demanding quantum tasks, such as long-distance QKD distance [19, 34–36]. A summary of recent representative advancements in superconducting SPDs is presented in Table 1.

However, as illustrated in the table, the reliance on superconductors necessitates stringent operating conditions, specifically with extremely low temperatures. Furthermore, these systems often entail high technical complexity and cost, hindering scalable commercial deployment.

Table 1: Summary of recent representative performance benchmarks for state-of-the-art superconducting SPDs.

Year	Researchers (et al.)	Operation temperature	Detection efficiency	Dark count rate
2020	P. Hu [30]	2.10 K	95.0 %	0.5×10^{-5}
2021	J. Chang [31]	2.50 K	99.5 %	1.1×10^{-3}
2021	G. Z. Xu [32]	0.84 K	92.2 %	3.6×10^{-5}
2023	I. Craiciu [33]	0.90 K	78.0 %	1.0×10^{-7}
2024	I. Charaev [37]	20.0 K	7.60 %	1.0×10^{-3}

To address these limitations, we propose a design for SPDs that meets advanced performance requirements, and even potentially outperforms superconducting devices, while relying on accessible, non-superconducting technology suitable for room-temperature operation. The proposed method, termed the Enhanced SPD (ESPD) scheme, iteratively upgrades the performance of an existing SPD level by level. As a demonstration of its capability, the ESPD scheme can enhance a non-superconducting SPD designed 20 years ago [28] to one achieving a DE exceeding 95% and a DCR below 10^{-9} , thereby rivaling state-of-the-art devices. Our method not only provides a high-performance SPD design realizable with current (even commercial) technologies but also establishes a general framework for engineering high-performance SPDs using low-technology components. This opens a new avenue for research into SPDs and related quantum optical technologies.

2 Results

In this section, we detail the architecture of the Enhanced Single-Photon Detector (ESPD) scheme, which iteratively improves performance starting from a base (existing) SPD. Then we establish the theoretical framework governing its operation and provide analytical approximations to characterize its performance.

2.1 Design of the Enhanced Single-Photon Detector

The ESPD architecture is designed to upgrade the capabilities of a given SPD level by level, ultimately achieving high DE and low DCR.

For clarity, we define the DE as the probability of generating a positive detection event given a single-photon input, and the DCR as the probability of a positive report given a vacuum input. Let ESPD_s denote the ESPD at level s , with DE η_s and DCR d_s . The iteration begins with an initial detector, ESPD_0 , characterized by $\eta_0 = \eta$ and $d_0 = d$.

The design utilizes qubit logic. The schematic of the ESPD paradigm is illustrated in Fig. 1.

The construction of the $(s+1)$ -th level detector, ESPD_{s+1} , proceeds as follows. To facilitate understanding, readers can consider an implementation where the degree of freedom (DOF) is photon polarization and the controlled operations are C-NOT gates.

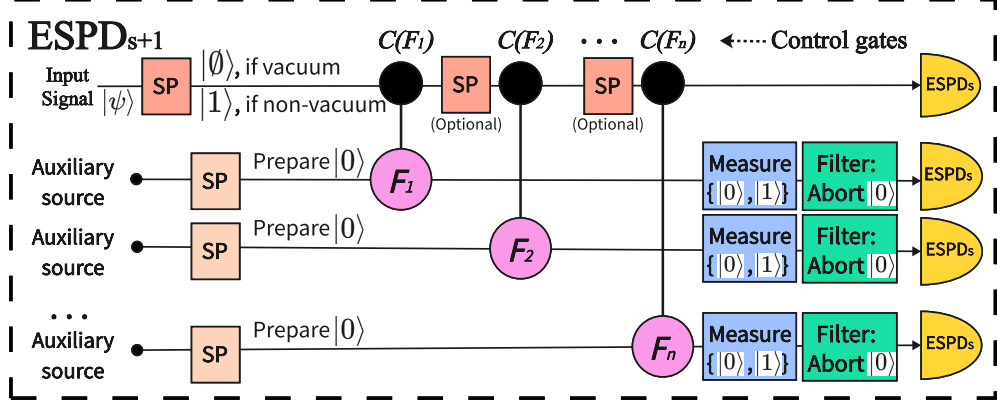


Fig. 1: Schematic representation of the recursive ESPD architecture. The $(s + 1)$ -th level detector (ESPD_{s+1}) is constructed by integrating multiple copies of the s -th level detector (ESPD_s) with controlled gates. Here, $C(F_i)$ are controlled gates, SP are state-preparation operations, measurements are projective measurements via basis $\{|0\rangle, |1\rangle\}$, and filters represent that the $|0\rangle$ path is aborted.

1. **DOF Selection:** Select a manipulable DOF of the incoming photon (e.g., polarization). Let $\{|0\rangle, |1\rangle\}$ be the computational basis for this DOF. We treat the signal as a qutrit in the basis $\{|\emptyset\rangle, |0\rangle, |1\rangle\}$, where $|\emptyset\rangle$ denotes the vacuum state, and $|0\rangle, |1\rangle$ denote the orthonormal states of a non-vacuum photon. Note that if the selected DOF is the photon number itself, $|0\rangle$ coincides with $|\emptyset\rangle$ and $|1\rangle$ represents non-vacuum. However, for practical implementations, it is often more convenient to use an internal DOF like polarization distinct from it.
2. **State Preparation:** Apply a state preparation operation to the incoming signal to initialize the selected DOF to $|1\rangle$. Consequently, a non-vacuum signal is mapped to $|1\rangle$, while a vacuum signal remains $|\emptyset\rangle$.
3. **Controlled Operations:** Implement n_{s+1} controlled operations, denoted as $C(F_i)$ for $i = 1, \dots, n_{s+1}$ (typically C-NOT gates). These gates interact the signal path with n_{s+1} auxiliary sources, each initialized in the state $|0\rangle$.
4. **Auxiliary Measurement:** Perform projective measurements on the auxiliary outputs in the basis $\{|0\rangle, |1\rangle\}$. Outcome paths of $|0\rangle$ are discarded, and only the $|1\rangle$ paths are preserved for detection.
5. **Detection:** Detect the signals at the end of paths, including the signal one and the auxiliary ones, using s -th level detectors, ESPD_s .
6. **Decision Logic:** A positive detection report for ESPD_{s+1} is generated if and only if at least k_{s+1} positive detections are registered among the $n_{s+1} + 1$ detectors (comprising n_{s+1} auxiliary detectors and one signal path detector). Otherwise, a negative report is returned. Here, k_{s+1} is a pre-selected threshold integer. Here, n_{s+1} should refer to the number of effective operations that survive post-selection (if the controlled gates include such), namely, the decision logic is essentially that the positive report rate on the multiple detections reaches a pre-defined threshold.

2.2 Theoretical Formulation

2.2.1 Notations

We define the parameters governing the system dynamics. As stated, η_s and d_s represent the DE and DCR of ESPD_s, respectively. Although η_s may theoretically depend on the photon number distribution, we approximate it as a unified value for the given system. The parameters n_{s+1} and k_{s+1} denote the number of effective controlled gates and the decision threshold for ESPD_{s+1}, respectively.

We assume all controlled operations $C(F_i)$ are identical, denoted simply as $C(F)$ for convenience. Let p be the transmission probability of the signal path through a single module (an optional state preparation followed by a $C(F)$). Specifically, p is the probability that the output signal remains non-vacuum given a non-vacuum input, accounting for loss but irrespective of decoherence (since the state can be re-prepared). Furthermore, let Q represent the intrinsic error rate of the auxiliary path in the absence of $C(F)$ (i.e., errors from auxiliary state preparation and measurement, but not including detection). Given the maturity of commercial linear optical components, we assume $Q \ll 1$ (typically $Q < 10^{-3}$). Finally, let P and Q denote the probabilities of obtaining a non-vacuum output on the controlled path before detection, given that the input to the corresponding module was non-vacuum or vacuum, respectively. For simplicity, we approximately assume p , P , and Q are invariant across all $C(F)$ operations.

2.2.2 Assumptions

In practical scenarios, SPD DE typically ranges from 10% to 90%, while the DCR is generally below 10^{-3} . Consequently, the hierarchy $0 \leq d \ll \eta \leq 1$ holds. We further assume $d_s \ll P\eta_s$. This condition is trivial, for if it were violated, the signal contribution from the controlled operations would be indistinguishable from device noise, rendering the operations practically insignificant. Additionally, the transmission rate is assumed to be $p \approx 1$ (see Section 3.1). Finally, considering practical implementation costs, we assume n_s and k_s are moderate integers satisfying $1 \leq k_s \leq n_s$.

2.2.3 Formulations

Let P_s and Q_s denote the probabilities of obtaining a positive report on an auxiliary path given a non-vacuum or vacuum input to the $C(F)$ module, respectively, using ESPD_s as the detector. These are expressed as:

$$P_{s+1} = P[\eta_s + (1 - \eta_s)d_s] + (1 - P)d_s = P\eta_s(1 - d_s) + d_s \approx P\eta_s \quad (1)$$

$$Q_{s+1} = Q[\eta_s + (1 - \eta_s)d_s] + (1 - Q)d_s = Q\eta_s(1 - d_s) + d_s \approx Q\eta_s + d_s \leq Q + d_s \quad (2)$$

Similarly, let P'_s and Q'_s denote the probabilities of obtaining a positive report on the signal path after all $C(F)$ operations, given a non-vacuum or vacuum output from the final gate, respectively, then:

$$P'_{s+1} = \eta_s + (1 - \eta_s)d_s \approx \eta_s, \quad Q'_{s+1} = d_s \quad (3)$$

We now derive the DE and DCR for the $(s+1)$ -th level.

For the DE calculation, we assume a non-vacuum input and calculate the probability of obtaining at least k_{s+1} positive reports out of $n_{s+1} + 1$ total detections. If the photon is lost exactly after the i -th $C(F)$, the probability of a final positive report is:

$$\begin{aligned}
& P_{s+1, k_{s+1}, i} \\
&= (1 - Q'_{s+1}) \sum_{j_1 + j_2 = k_{s+1}}^{n_{s+1}} \binom{i}{j_1} P_{s+1}^{j_1} (1 - P_{s+1})^{i-j_1} \binom{n-i}{j_2} Q_{s+1}^{j_2} (1 - Q_{s+1})^{n-i-j_2} \\
&+ Q'_{s+1} \sum_{j_1 + j_2 = k_{s+1} - 1}^{n_{s+1}} \binom{i}{j_1} P_{s+1}^{j_1} (1 - P_{s+1})^{i-j_1} \binom{n-i}{j_2} Q_{s+1}^{j_2} (1 - Q_{s+1})^{n-i-j_2}
\end{aligned} \tag{4}$$

where the first and second terms correspond to scenarios where the signal path detector reports negative or positive, respectively.

If the photon survives all $C(F)$ operations, the probability is:

$$\begin{aligned}
P_{s+1, k_{s+1}} &= P'_{s+1} \sum_{j \geq k_{s+1} - 1}^{n_{s+1}} \binom{n_{s+1}}{j} P_{s+1}^j (1 - P_{s+1})^{n_{s+1} - j} \\
&+ (1 - P'_{s+1}) \sum_{j \geq k_{s+1}}^{n_{s+1}} \binom{n_{s+1}}{j} P_{s+1}^j (1 - P_{s+1})^{n_{s+1} - j} \\
&= P'_{s+1} \binom{n_{s+1}}{k_{s+1} - 1} P_{s+1}^{k_{s+1} - 1} (1 - P_{s+1})^{n_{s+1} - k_{s+1} + 1} \\
&+ \sum_{j \geq k_{s+1}}^{n_{s+1}} \binom{n_{s+1}}{j} P_{s+1}^j (1 - P_{s+1})^{n_{s+1} - j}
\end{aligned} \tag{5}$$

Combining these, the DE of ESPD $_{s+1}$ is:

$$\eta_{s+1} = p^{n_{s+1}} P_{s+1, k_{s+1}} + \sum_{i=1}^{n_{s+1}} p^{i-1} (1 - p) P_{s+1, k_{s+1}, i} \tag{6}$$

For the DCR calculation, we assume a vacuum input. The probability of a false positive is:

$$\begin{aligned}
d_{s+1} &= (1 - Q'_{s+1}) \sum_{j \geq k_{s+1}}^{n_{s+1}} \binom{n_{s+1}}{j} Q_{s+1}^j (1 - Q_{s+1})^{n_{s+1} - j} \\
&+ Q'_{s+1} \sum_{j \geq k_{s+1} - 1}^{n_{s+1}} \binom{n_{s+1}}{j} Q_{s+1}^j (1 - Q_{s+1})^{n_{s+1} - j}
\end{aligned} \tag{7}$$

Collectively, the DE and DCR evolution is governed by the non-linear time-variant dynamic system:

$$(\eta_{s+1}, d_{s+1}) = G_{s+1}(\eta_s, d_s), (\eta_0, d_0) = (\eta, d) \quad (8)$$

where the mapping G is defined by Eq. (1) to (7).

2.3 Analytical Approximation and Stability Analysis

While Eq. (8) describes the exact dynamics, an analytical solution is generally intractable. However, employing the approximations in Eq. (1) to (3) and the assumptions from Section 2.2.2, we can derive simplified bounds to elucidate the system's behavior.

Consider the DCR evolution. Eq. (7) can be reformulated as:

$$d_{s+1} = Q'_{s+1} \binom{n_{s+1}}{k_{s+1}-1} Q_{s+1}^{k-1} (1 - Q_{s+1})^{n_{s+1}-k_{s+1}+1} + \sum_{j \geq k_{s+1}} \binom{n_{s+1}}{j} Q_{s+1}^j (1 - Q_{s+1})^{n_{s+1}-j} \quad (9)$$

Proposition 1 Define the function

$$f(x) = a \binom{n}{k-1} x^{k-1} (1-x)^{n-k+1} + \sum_{j \geq k} \binom{n}{j} x^j (1-x)^{n-j} \quad (10)$$

Then $f(x)$ is monotonically increasing for $x \in [0, \frac{k-1}{n}]$.

Proof: For $x \in [0, \frac{k-1}{n}]$:

$$\begin{aligned} & \frac{d}{dx} f(x) \\ &= x^{k-2} \left[\binom{n}{k-1} a (1-x)^{n-k} [(k-1)(1-x) - x(n-k+1)] \right. \\ & \quad \left. + \sum_{j \geq k} \binom{n}{j} [j x^{j+1-k} (1-x)^{n-j} - x^{j-k+2} (1-x)^{n-j-1} (n-j)] \right] \\ &= x^{k-2} \left[\binom{n}{k-1} a (1-x)^{n-k} (k-1-nx) + \sum_{j \geq k} \binom{n}{j} x^{j+1-k} (1-x)^{n-j-1} (j-nx) \right] \\ &\geq x^{k-2} \left[\binom{n}{k-1} a (1-x)^{n-k} + \sum_{j \geq k} \binom{n}{j} x^{j+1-k} (1-x)^{n-j-1} \right] (k-1-nx) \geq 0 \end{aligned} \quad (11)$$

■

Applying the upper bound from Eq. (2), substituting Eq. (3) to Eq. (9), and assuming $k - 1 \geq nx$, we obtain:

$$d_{s+1} \leq d_s \binom{n_{s+1}}{k_{s+1} - 1} (Q + d_s)^{k_{s+1} - 1} (1 - Q - d_s)^{n_{s+1} - k_{s+1} + 1} + \sum_{j \geq k_{s+1}} \binom{n_{s+1}}{j} (Q + d_s)^j (1 - Q - d_s)^{n_{s+1} - j} \quad (12)$$

which is notably independent of η_s . Given $Q_s, d_s \ll 1$ and moderate n_{s+1}, k_{s+1} , we assume $\binom{n_{s+1}}{j} (Q + d_s) \ll 1$. This yields the approximation:

$$\begin{aligned} d_{s+1} &\lesssim d_s \binom{n_{s+1}}{k_{s+1} - 1} (Q + d_s)^{k_{s+1} - 1} + \binom{n_{s+1}}{k_{s+1}} (Q + d_s)^{k_{s+1}} \\ &= (Q + d_s)^{k_{s+1} - 1} \left[(d_s \binom{n_{s+1}}{k_{s+1} - 1} + \binom{n_{s+1}}{k_{s+1}} (Q + d_s) \right] \end{aligned} \quad (13)$$

This provides an estimation for the DCR at level $s + 1$.

Similarly, the DE can be lower-bounded by:

$$\begin{aligned} \eta_{s+1} &\geq p^{n_{s+1}} [P'_{s+1} \sum_{j \geq k_{s+1} - 1} \binom{n_{s+1}}{j} P_{s+1}^j (1 - P_{s+1})^{n_{s+1} - j} \\ &\quad + (1 - P'_{s+1}) \sum_{j \geq k_{s+1}} \binom{n_{s+1}}{j} P_{s+1}^j (1 - P_{s+1})^{n_{s+1} - j}] \\ &= p^{n_{s+1}} [P'_{s+1} \binom{n_{s+1}}{k_{s+1} - 1} P_{s+1}^{k_{s+1} - 1} (1 - P_{s+1})^{n_{s+1} - k_{s+1} + 1} \\ &\quad + \sum_{j \geq k_{s+1}} \binom{n_{s+1}}{j} P_{s+1}^j (1 - P_{s+1})^{n_{s+1} - j}] \\ &\approx p^{n_{s+1}} [\eta_s \binom{n_{s+1}}{k_{s+1} - 1} (P\eta_s)^{k_{s+1} - 1} (1 - P\eta_s)^{n_{s+1} - k_{s+1} + 1} \\ &\quad + \sum_{j \geq k_{s+1}} \binom{n_{s+1}}{j} (P\eta_s)^j (1 - P\eta_s)^{n_{s+1} - j}] \end{aligned} \quad (14)$$

which is independent of d_s . Therefore, solving the inequality

$$p^n (Px)^{k-1} \left[x \binom{n}{k-1} (1 - Px)^{n-k+1} + \sum_{j \geq k} \binom{n}{j} (Px)^{j-k+1} (1 - Px)^{n-j} \right] - x > 0 \quad (15)$$

determines the condition under which the DE is enhanced in the subsequent level. If n_s and k_s are constant across levels and the system is stable, the DE of ESPD_s will converge to a root of the left-hand side of Eq. (15).

2.4 Performance Simulations

While obtaining an exact analytical solution for the non-linear, time-variant dynamic system governing the ESPD is mathematically complex, numerical methods provide a robust and sufficient approach for practical design. In this section, we present numerical simulations to validate the ESPD paradigm, demonstrating that substantial performance gains are achievable even with moderate initial hardware specifications. For example, a three-level ESPD can transform a semiconductor SPD into one exhibiting $DE > 95\%$ and $DCR < 10^{-9}$, effectively removing the necessity for superconducting materials while matching or exceeding the performance of state-of-the-art SNSPDs.

Simulation Parameters: We evaluated the ESPD scheme using two baseline detectors: one representing older technology with $(\eta_0, d_0) = (59\%, 10^{-2})$ [28], and another representing typical InGaAs/InP performance with $(\eta_0, d_0) = (27.5\%, 10^{-6})$ [29]. The transmission probability is set to $p = 0.99$, and the auxiliary path error rate $Q = 0.2\%$ (see Section 3.1). We considered two controlled gate fidelity scenarios: $P = 0.81$, representing standard linear optical C-NOT gates [38], and $P = 0.95^1$, representing high-fidelity implementations [39, 40]. Also, a further implementation with P reduced to 0.4 is reported in Section 3.1. Various combinations of the configuration parameters n_s and k_s are evaluated.

Performance Outcomes: Table 2 to 5 and Fig. 2 to 5 summarize the achievable performance metrics across varying configurations and baseline architectures. The results indicate that the ESPD scheme significantly enhances the capabilities of conventional SPDs. Notably, with only three levels of enhancement, the detectors achieve performance metrics ($DE > 95\%$, $DCR < 10^{-9}$) that rival or surpass those of advanced superconducting SPDs.

3 Discussion

We now discuss the device requirements, potential applications, as well as current limitations and avenues for future work.

3.1 Device Requirements

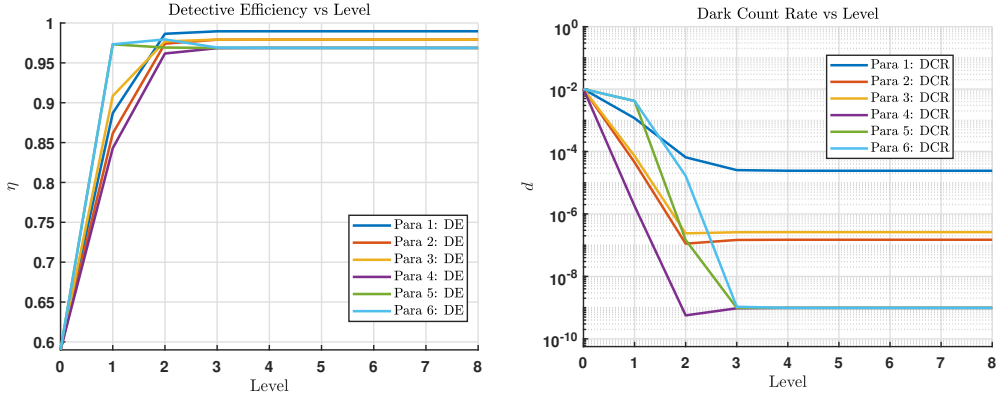
The flexibility of the ESPD paradigm, which allows for various DOF to be employed, enables the selection of an easily manipulated parameter. In practical implementations, this facilitates state preparation and projective measurement, ensuring that the error parameter Q can be executed with extremely low rates. Specifically, Q can be suppressed to below the 10^{-4} level using commercial platforms[41, 42], thereby guaranteeing condition $Q \ll 1$.

The primary technological requirements of the ESPD scheme are the controlled quantum gates, typically C-NOT operations, which define the critical parameters p and P . In practice, the transmission rate p is often approximated as $p \approx 1$, representing a high transmission efficiency [42–49]. However, since p decays exponentially as the

¹Corresponding to about 0.22 dB, which is very likely to be achieved commercially in the short term, since it is confident to achieve by the commercial platform Q.ANT in 2026.

Table 2: Performance evolution of an ESPD initialized with a baseline detector from [28], with $\eta_0 = 59\%$, $d_0 = 10^{-2}$, and high controlled gate fidelity, $P = 0.99$.

	Para 1		Para 2		Para 3	
Level	(n, k)	(DE (η), DCR (d))	(n, k)	(DE (η), DCR (d))	(n, k)	(DE (η), DCR (d))
0	-	(59.0%, 1.0 × 10 ⁻²)	-	(59.0%, 1.0 × 10 ⁻²)	-	(59.0%, 1.0 × 10 ⁻²)
1	(4,2)	(88.7%, 1.2 × 10 ⁻³)	(6,3)	(86.2%, 4.5 × 10 ⁻⁵)	(7,3)	(90.9%, 7.2 × 10 ⁻⁵)
2	(4,2)	(98.6%, 6.5 × 10 ⁻⁵)	(6,3)	(97.4%, 1.1 × 10 ⁻⁸)	(7,3)	(97.7%, 2.4 × 10 ⁻⁷)
3	(4,2)	(99.0%, 2.5 × 10 ⁻⁵)	(6,3)	(97.9%, 1.5 × 10 ⁻⁷)	(7,3)	(97.9%, 2.6 × 10 ⁻⁷)
4	(4,2)	(99.0%, 2.4 × 10 ⁻⁵)	(6,3)	(97.9%, 1.5 × 10 ⁻⁷)	(7,3)	(97.9%, 2.6 × 10 ⁻⁷)
5	(4,2)	(99.0%, 2.4 × 10 ⁻⁵)	(6,3)	(97.9%, 1.5 × 10 ⁻⁷)	(7,3)	(97.9%, 2.6 × 10 ⁻⁷)
6	(4,2)	(99.0%, 2.4 × 10 ⁻⁵)	(6,3)	(97.9%, 1.5 × 10 ⁻⁷)	(7,3)	(97.9%, 2.6 × 10 ⁻⁷)
7	(4,2)	(99.0%, 2.4 × 10 ⁻⁵)	(6,3)	(97.9%, 1.5 × 10 ⁻⁷)	(7,3)	(97.9%, 2.6 × 10 ⁻⁷)
8	(4,2)	(99.0%, 2.4 × 10 ⁻⁵)	(6,3)	(97.9%, 1.5 × 10 ⁻⁷)	(7,3)	(97.9%, 2.6 × 10 ⁻⁷)
	Para 4		Para 5		Para 6	
Level	(n, k)	(DE (η), DCR (d))	(n, k)	(DE (η), DCR (d))	(n, k)	(DE (η), DCR (d))
0	-	(59.0%, 1.0 × 10 ⁻²)	-	(59.0%, 1.0 × 10 ⁻²)	-	(59.0%, 1.0 × 10 ⁻²)
1	(8,4)	(84.3%, 1.8 × 10 ⁻⁶)	(8,2)	(97.3%, 4.2 × 10 ⁻³)	(8,2)	(97.3%, 4.2 × 10 ⁻³)
2	(8,4)	(96.2%, 5.7 × 10 ⁻¹⁰)	(8,4)	(96.9%, 1.5 × 10 ⁻⁷)	(8,3)	(97.9%, 1.7 × 10 ⁻⁵)
3	(8,4)	(96.8%, 9.5 × 10 ⁻¹⁰)	(8,4)	(96.9%, 9.8 × 10 ⁻¹⁰)	(8,4)	(96.9%, 1.1 × 10 ⁻⁹)
4	(8,4)	(96.9%, 9.8 × 10 ⁻¹⁰)	(8,4)	(96.9%, 9.8 × 10 ⁻¹⁰)	(8,4)	(96.9%, 9.8 × 10 ⁻¹⁰)
5	(8,4)	(96.9%, 9.8 × 10 ⁻¹⁰)	(8,4)	(96.9%, 9.8 × 10 ⁻¹⁰)	(8,4)	(96.9%, 9.8 × 10 ⁻¹⁰)
6	(8,4)	(96.9%, 9.8 × 10 ⁻¹⁰)	(8,4)	(96.9%, 9.8 × 10 ⁻¹⁰)	(8,4)	(96.9%, 9.8 × 10 ⁻¹⁰)
7	(8,4)	(96.9%, 9.8 × 10 ⁻¹⁰)	(8,4)	(96.9%, 9.8 × 10 ⁻¹⁰)	(8,4)	(96.9%, 9.8 × 10 ⁻¹⁰)
8	(8,4)	(96.9%, 9.8 × 10 ⁻¹⁰)	(8,4)	(96.9%, 9.8 × 10 ⁻¹⁰)	(8,4)	(96.9%, 9.8 × 10 ⁻¹⁰)



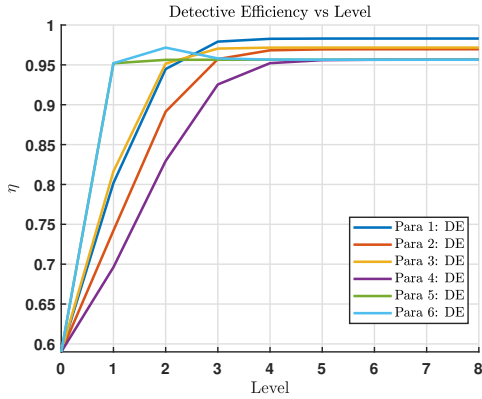
(a) Detection efficiency η_s vs. level s for varying (n_s, k_s) .

(b) Dark count rate d_s vs. level s for varying (n_s, k_s) .

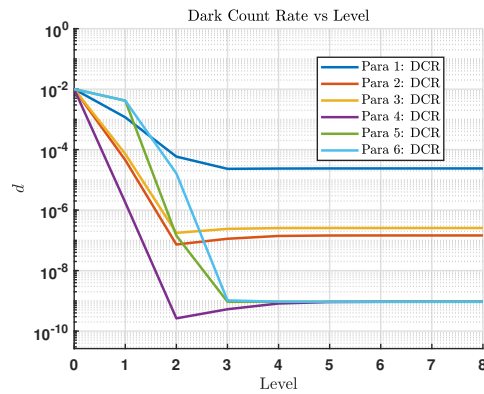
Fig. 2: Performance scaling for initial parameters $\eta_0 = 59.0\%$, $d_0 = 1.0 \times 10^{-2}$, with $P = 0.99$.

Table 3: Performance evolution of an ESPD initialized with a baseline detector from [28], with $\eta_0 = 59\%$, $d_0 = 10^{-2}$, and moderate controlled gate fidelity, $P = 0.81$.

Para 1			Para 2			Para 3		
Level	(n, k)	(DE (η), DCR (d))	(n, k)	(DE (η), DCR (d))	(n, k)	(DE (η), DCR (d))	(n, k)	(DE (η), DCR (d))
0	-	(59.0%, 1.0×10^{-2})	-	(59.0%, 1.0×10^{-2})	-	(59.0%, 1.0×10^{-2})	-	(59.0%, 1.0×10^{-2})
1	(4,2)	(80.2%, 1.2×10^{-3})	(6,3)	(74.2%, 4.5×10^{-5})	(7,3)	(81.6%, 7.2×10^{-5})	(7,3)	(81.6%, 7.2×10^{-5})
2	(4,2)	(94.5%, 5.9×10^{-5})	(6,3)	(89.1%, 7.3×10^{-8})	(7,3)	(95.2%, 1.8×10^{-7})	(7,3)	(95.2%, 1.8×10^{-7})
3	(4,2)	(97.9%, 2.3×10^{-5})	(6,3)	(95.7%, 1.1×10^{-7})	(7,3)	(97.0%, 2.4×10^{-7})	(7,3)	(97.0%, 2.4×10^{-7})
4	(4,2)	(98.3%, 2.4×10^{-5})	(6,3)	(96.8%, 1.4×10^{-7})	(7,3)	(97.2%, 2.5×10^{-7})	(7,3)	(97.2%, 2.5×10^{-7})
5	(4,2)	(98.3%, 2.4×10^{-5})	(6,3)	(96.9%, 1.4×10^{-7})	(7,3)	(97.2%, 2.6×10^{-7})	(7,3)	(97.2%, 2.6×10^{-7})
6	(4,2)	(98.3%, 2.4×10^{-5})	(6,3)	(97.0%, 1.5×10^{-7})	(7,3)	(97.2%, 2.6×10^{-7})	(7,3)	(97.2%, 2.6×10^{-7})
7	(4,2)	(98.3%, 2.4×10^{-5})	(6,3)	(97.0%, 1.5×10^{-7})	(7,3)	(97.2%, 2.6×10^{-7})	(7,3)	(97.2%, 2.6×10^{-7})
8	(4,2)	(98.3%, 2.4×10^{-5})	(6,3)	(97.0%, 1.5×10^{-7})	(7,3)	(97.2%, 2.6×10^{-7})	(7,3)	(97.2%, 2.6×10^{-7})
Para 4			Para 5			Para 6		
Level	(n, k)	(DE (η), DCR (d))	(n, k)	(DE (η), DCR (d))	(n, k)	(DE (η), DCR (d))	(n, k)	(DE (η), DCR (d))
0	-	(59.0%, 1.0×10^{-2})	-	(59.0%, 1.0×10^{-2})	-	(59.0%, 1.0×10^{-2})	-	(59.0%, 1.0×10^{-2})
1	(8,4)	(69.6%, 1.8×10^{-6})	(8,2)	(95.2%, 4.2×10^{-3})	(8,2)	(95.2%, 4.2×10^{-3})	(8,2)	(95.2%, 4.2×10^{-3})
2	(8,4)	(82.9%, 2.6×10^{-10})	(8,4)	(95.6%, 1.4×10^{-7})	(8,3)	(97.2%, 1.6×10^{-5})	(8,3)	(97.2%, 1.6×10^{-5})
3	(8,4)	(92.5%, 5.3×10^{-10})	(8,4)	(95.6%, 9.3×10^{-10})	(8,4)	(95.8%, 1.0×10^{-9})	(8,4)	(95.8%, 1.0×10^{-9})
4	(8,4)	(95.2%, 8.2×10^{-10})	(8,4)	(95.6%, 9.3×10^{-10})	(8,4)	(95.7%, 9.4×10^{-10})	(8,4)	(95.7%, 9.4×10^{-10})
5	(8,4)	(95.6%, 9.1×10^{-10})	(8,4)	(95.6%, 9.3×10^{-10})	(8,4)	(95.6%, 9.3×10^{-10})	(8,4)	(95.6%, 9.3×10^{-10})
6	(8,4)	(95.6%, 9.3×10^{-10})	(8,4)	(95.6%, 9.3×10^{-10})	(8,4)	(95.6%, 9.3×10^{-10})	(8,4)	(95.6%, 9.3×10^{-10})
7	(8,4)	(95.6%, 9.3×10^{-10})	(8,4)	(95.6%, 9.3×10^{-10})	(8,4)	(95.6%, 9.3×10^{-10})	(8,4)	(95.6%, 9.3×10^{-10})
8	(8,4)	(95.6%, 9.3×10^{-10})	(8,4)	(95.6%, 9.3×10^{-10})	(8,4)	(95.6%, 9.3×10^{-10})	(8,4)	(95.6%, 9.3×10^{-10})



(a) Detection efficiency η_s vs. level s for varying (n_s, k_s) .

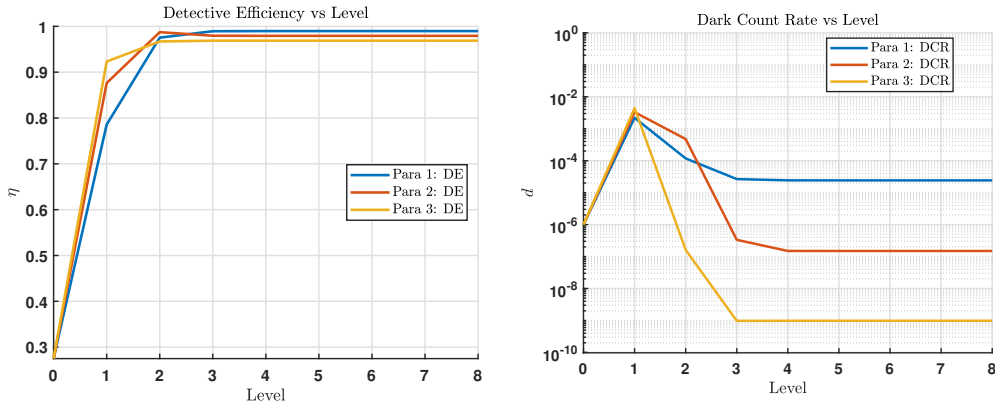


(b) Dark count rate d_s vs. level s for varying (n_s, k_s) .

Fig. 3: Performance scaling for initial parameters $\eta_0 = 59.0\%$, $d_0 = 1.0 \times 10^{-2}$, with $P = 0.81$.

Table 4: Performance evolution of an ESPD initialized with a baseline detector from [29], with $\eta_0 = 27.5\%$, $d_0 = 10^{-6}$, and high controlled gate fidelity, $P = 0.99$.

	Para 1		Para 2		Para 3	
Level	(n, k)	(DE (η), DCR (d))	(n, k)	(DE (η), DCR (d))	(n, k)	(DE (η), DCR (d))
0	-	(27.5%, 1.0×10^{-6})	-	(27.5%, 1.0×10^{-6})	-	(27.5%, 1.0×10^{-6})
1	(4,1)	(78.6%, 2.2×10^{-3})	(6,1)	(87.6%, 3.3×10^{-3})	(8,1)	(92.3%, 4.4×10^{-3})
2	(4,2)	(97.5%, 1.2×10^{-4})	(6,2)	(98.7%, 4.7×10^{-4})	(8,4)	(96.7%, 1.6×10^{-7})
3	(4,2)	(98.9%, 2.7×10^{-5})	(6,3)	(98.0%, 3.7×10^{-7})	(8,4)	(96.9%, 9.7×10^{-10})
4	(4,2)	(99.0%, 2.4×10^{-5})	(6,3)	(97.9%, 1.5×10^{-7})	(8,4)	(96.9%, 9.8×10^{-10})
5	(4,2)	(99.0%, 2.4×10^{-5})	(6,3)	(97.9%, 1.5×10^{-7})	(8,4)	(96.9%, 9.8×10^{-10})
6	(4,2)	(99.0%, 2.4×10^{-5})	(6,3)	(97.9%, 1.5×10^{-7})	(8,4)	(96.9%, 9.8×10^{-10})
7	(4,2)	(99.0%, 2.4×10^{-5})	(6,3)	(97.9%, 1.5×10^{-7})	(8,4)	(96.9%, 9.8×10^{-10})
8	(4,2)	(99.0%, 2.4×10^{-5})	(6,3)	(97.9%, 1.5×10^{-7})	(8,4)	(96.9%, 9.8×10^{-10})



(a) Detection efficiency η_s vs. level s for varying (n_s, k_s) .

(b) Dark count rate d_s vs. level s for varying (n_s, k_s) .

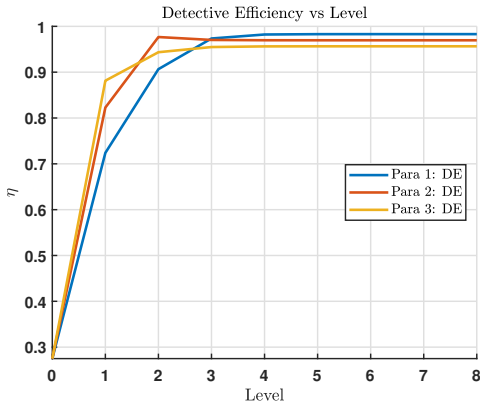
Fig. 4: Performance scaling for initial parameters $\eta_0 = 27.5\%$, $d_0 = 1.0 \times 10^{-6}$, with $P = 0.99$.

number of stages n increases, experimental characterization of p remains crucial. Table 6 and Fig. 6 demonstrate the performance when p is degraded, showing that the ESPD framework remains valid even if p drops to 0.86, albeit with reduced performance compared to higher values.

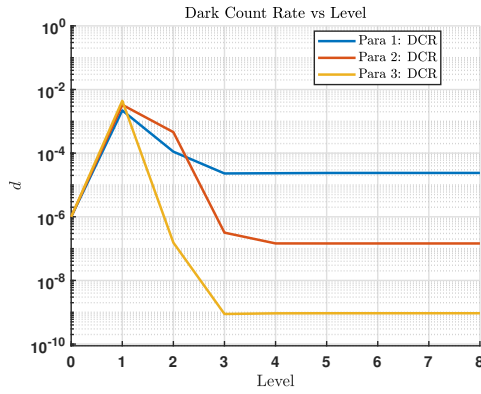
Attention now shifts to the parameter P , which is intrinsically linked to the fidelity of the C-NOT gate. Notably, P is lower-bounded by the gate's overall fidelity, as P quantifies deviation only on the controlled path, whereas the full C-NOT fidelity accounts for the correct operation rate of both the control and controlled paths. Contemporary C-NOT gates demonstrate high fidelities, exceeding 99% [39, 40] using modern technology and reaching 81% via linear-optical methods [38], suggesting that

Table 5: Performance evolution of an ESPD initialized with a baseline detector from [29], with $\eta_0 = 27.5\%$, $d_0 = 10^{-6}$, and moderate controlled gate fidelity, $P = 0.81$.

	Para 1		Para 2		Para 3	
Level	(n, k)	(DE (η), DCR (d))	(n, k)	(DE (η), DCR (d))	(n, k)	(DE (η), DCR (d))
0	-	(27.5%, 1.0×10^{-6})	-	(27.5%, 1.0×10^{-6})	-	(27.5%, 1.0×10^{-6})
1	(4,1)	(72.4%, 2.2×10^{-3})	(6,1)	(82.3%, 3.3×10^{-3})	(8,1)	(88.1%, 4.4×10^{-3})
2	(4,2)	(90.7%, 1.1×10^{-4})	(6,2)	(97.7%, 4.6×10^{-4})	(8,4)	(94.4%, 1.5×10^{-7})
3	(4,2)	(97.3%, 2.3×10^{-5})	(6,3)	(97.0%, 3.2×10^{-7})	(8,4)	(95.5%, 8.8×10^{-10})
4	(4,2)	(98.2%, 2.3×10^{-5})	(6,3)	(97.0%, 1.5×10^{-7})	(8,4)	(95.6%, 9.3×10^{-10})
5	(4,2)	(98.3%, 2.4×10^{-5})	(6,3)	(97.0%, 1.5×10^{-7})	(8,4)	(95.6%, 9.3×10^{-10})
6	(4,2)	(98.3%, 2.4×10^{-5})	(6,3)	(97.0%, 1.5×10^{-7})	(8,4)	(95.6%, 9.3×10^{-10})
7	(4,2)	(98.3%, 2.4×10^{-5})	(6,3)	(97.0%, 1.5×10^{-7})	(8,4)	(95.6%, 9.3×10^{-10})
8	(4,2)	(98.3%, 2.4×10^{-5})	(6,3)	(97.0%, 1.5×10^{-7})	(8,4)	(95.6%, 9.3×10^{-10})



(a) Detection efficiency η_s vs. level s for varying (n_s, k_s) .



(b) Dark count rate d_s vs. level s for different (n_s, k_s) .

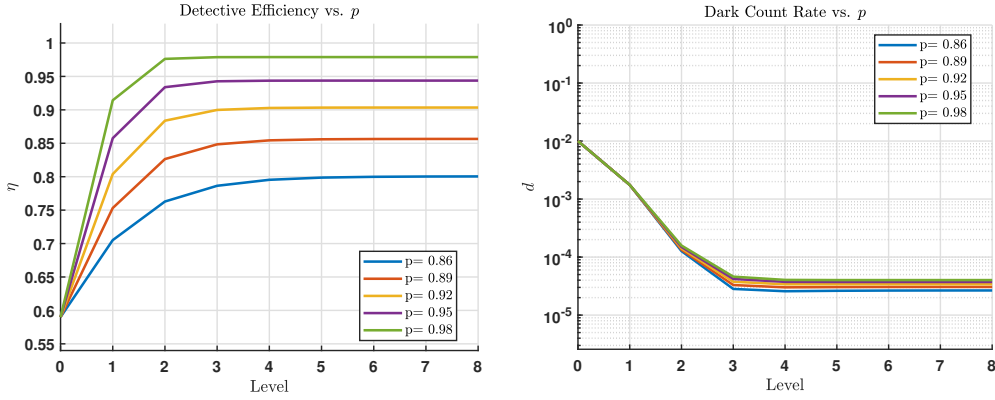
Fig. 5: Performance scaling for initial parameters $\eta_0 = 27.5\%$, $d_0 = 1.0 \times 10^{-6}$, with $P = 0.81$.

high values of P are readily attainable. Our numerical results in Section 2.4 confirm that the ESPD paradigm does not rely on an excessively demanding value for P , showing similar substantial performance gains for $P = 0.99$ and $P = 0.81$. Furthermore, Table 7 and Fig. 7 illustrate the robustness of the scheme, confirming its efficacy even when the C-NOT fidelity parameter is severely degraded to $P = 0.40$. This demonstrated robustness confirms that the technological demands of the ESPD method are fully compatible with existing quantum technologies.

It is also important to note that the implementation of the ESPD scheme does not require perfect auxiliary photon sources. The parameter P relies solely on the detection of the state $|1\rangle$ from the auxiliary path when the control signal input is non-vacuum.

Table 6: Performance evolution of an ESPD initialized with a baseline detector from [28], with p varied from 0.86 to 0.98. Here, $P = 0.99$ and experiments are run for $(n, k) = (5, 2)$ on each level.

	$p=0.86$	$p=0.89$	$p=0.92$	$p=0.95$	$p=0.98$
Level	(DE (η), DCR (d))	(DE (η), DCR (d))	(DE (η), DCR (d))	(DE (η), DCR (d))	(DE (η), DCR (d))
0	(59.0%, 1.0×10^{-2})	(59.0%, 1.0×10^{-2})	(59.0%, 1.0×10^{-2})	(59.0%, 1.0×10^{-2})	(59.0%, 1.0×10^{-2})
1	(70.5%, 1.8×10^{-3})	(75.3%, 1.8×10^{-3})	(80.4%, 1.8×10^{-3})	(85.8%, 1.8×10^{-3})	(91.4%, 1.8×10^{-3})
2	(76.3%, 1.3×10^{-4})	(82.6%, 1.3×10^{-4})	(88.4%, 1.4×10^{-4})	(93.4%, 1.5×10^{-4})	(97.6%, 1.6×10^{-4})
3	(78.6%, 2.8×10^{-5})	(84.8%, 3.3×10^{-5})	(90.0%, 3.8×10^{-5})	(94.3%, 4.2×10^{-5})	(97.9%, 4.6×10^{-5})
4	(79.5%, 2.6×10^{-5})	(85.4%, 3.0×10^{-5})	(90.3%, 3.4×10^{-5})	(93.4%, 3.7×10^{-5})	(97.9%, 4.0×10^{-5})
5	(79.9%, 2.6×10^{-5})	(85.6%, 3.0×10^{-5})	(90.3%, 3.4×10^{-5})	(93.4%, 3.7×10^{-5})	(97.9%, 4.0×10^{-5})
6	(80.0%, 2.6×10^{-5})	(85.6%, 3.1×10^{-5})	(90.3%, 3.4×10^{-5})	(93.4%, 3.7×10^{-5})	(97.9%, 4.0×10^{-5})
7	(80.0%, 2.7×10^{-5})	(85.6%, 3.1×10^{-5})	(90.3%, 3.4×10^{-5})	(93.4%, 3.7×10^{-5})	(97.9%, 4.0×10^{-5})
8	(80.0%, 2.7×10^{-5})	(85.7%, 3.1×10^{-5})	(90.3%, 3.4×10^{-5})	(93.4%, 3.7×10^{-5})	(97.9%, 4.0×10^{-5})



(a) Detection efficiency η_s vs. p for $(n_s, k_s) = (5, 2)$. (b) Dark count rate d_s vs. level p for $(n_s, k_s) = (5, 2)$.

Fig. 6: Performance scaling for initial parameters $\eta_0 = 59.0\%$, $d_0 = 1.0 \times 10^{-2}$, with $P = 0.99$.

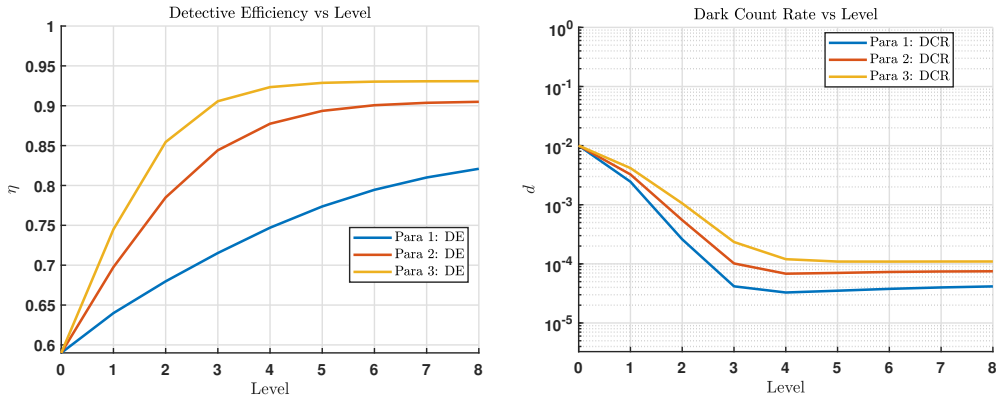
This condition holds true regardless of the exact number of photons in the auxiliary path or the presence of unwanted $|0\rangle$ measurement outcomes, which are inherently filtered out². Intuitively, multi-photon sources might even offer practical benefits over single-photon sources by providing more opportunities for detecting the required final $|1\rangle$, although a rigorous theoretical formulation of this potential advantage is reserved for future work.

Finally, the requirements for the initial single-photon detector (SPD) used for initialization are minimal. As demonstrated in Section 2.4, the stable performance of the ESPD is largely independent of the specific characteristics of the starting detector,

²This justifies the necessity of the dedicated filter block within the design.

Table 7: Performance evolution of an ESPD initialized with a baseline detector from [28], with $\eta_0 = 59\%$, $d_0 = 10^{-2}$, under a low controlled gate fidelity, $P = 0.40$.

Level	Para 1		Para 2		Para 3	
	(n, k)	(DE (η), DCR (d))	(n, k)	(DE (η), DCR (d))	(n, k)	(DE (η), DCR (d))
0	-	(59.0%, 1.0×10^{-2})	-	(59.0%, 1.0×10^{-2})	-	(59.0%, 1.0×10^{-2})
1	(6,2)	(64.0%, 2.4×10^{-3})	(7,2)	(69.8%, 3.3×10^{-3})	(8,2)	(74.5%, 4.2×10^{-3})
2	(6,2)	(68.0%, 2.6×10^{-4})	(7,2)	(78.5%, 5.5×10^{-4})	(8,2)	(85.5%, 1.1×10^{-3})
3	(6,2)	(71.5%, 4.2×10^{-5})	(7,2)	(84.4%, 1.0×10^{-4})	(8,2)	(90.6%, 2.3×10^{-4})
4	(6,2)	(74.7%, 3.3×10^{-5})	(7,2)	(87.7%, 6.8×10^{-5})	(8,2)	(92.3%, 1.2×10^{-4})
5	(6,2)	(77.4%, 3.5×10^{-5})	(7,2)	(89.4%, 7.0×10^{-5})	(8,2)	(92.9%, 1.1×10^{-4})
6	(6,2)	(79.5%, 3.8×10^{-5})	(7,2)	(90.1%, 7.3×10^{-5})	(8,2)	(93.0%, 1.1×10^{-4})
7	(6,2)	(81.0%, 4.0×10^{-5})	(7,2)	(90.4%, 7.4×10^{-5})	(8,2)	(93.1%, 1.1×10^{-4})
8	(6,2)	(82.1%, 4.2×10^{-5})	(7,2)	(90.5%, 7.5×10^{-5})	(8,2)	(93.1%, 1.1×10^{-4})



(a) Detection efficiency η_s vs. level s for varying (n_s, k_s) .

(b) Dark count rate d_s vs. level s for different (n_s, k_s) .

Fig. 7: Performance scaling for initial parameters $\eta_0 = 59.0\%$, $d_0 = 1.0 \times 10^{-2}$, with $P = 0.40$.

provided it falls within a certain convergence interval. The dynamic system described by Eq.(8) exhibits convergence to a stable operational point within this interval, irrespective of the initial point. Moreover, while a trade-off exists between DE and DCR, the DCR of the ESPD can be drastically reduced by increasing k , and the DE can be significantly enhanced by selecting a small k . One or two levels of the ESPD paradigm, using suitable n and k , can readily adjust the detector's performance to a desirable operational window, provided the initial SPD is not severely deficient. Indeed, simulations confirm that both an SPD with low DE and low DCR and one with moderate DE and high DCR serve as viable starting points. In summary, the ESPD scheme only

requires a normal, low-performance SPD for initialization, which is easily achieved. For instance, a device dating back two decades [28] is sufficient.

3.2 Applications

To illustrate the practical impact of the ESPD scheme, we consider its application in QKD. For a QKD protocol having a secure threshold e_{th} , the minimal tolerable channel transmission rate γ is conventionally approximated by:

$$\gamma = \frac{(1 - 2e_{th})d}{\eta[e_{th} - e_C + d(1 - 2e)]} \approx \frac{1 - 2e_{th}}{e_{th} - e_C} \frac{d}{\eta} \quad (16)$$

Given that the ESPD paradigm reduces the DCR (d) by several orders of magnitude, it proportionately lowers the minimal tolerable channel transmission rate γ by the same factor. Furthermore, the simultaneous enhancement of the DE (η) not only lowers γ but also translates directly into an improved QKD key rate at any fixed distance.

Compared to the empty-signal-detection paradigm [27], which also reduces the threshold of the minimal tolerable channel transmission rate, the ESPD scheme avoids introducing an extra sifting term that penalizes efficiency. This allows for significant QKD performance improvements without an additional efficiency cost. Consequently, the ESPD paradigm offers a compelling first-choice solution for practical quantum communication implementations.

3.3 Limitation and Future Work

Despite the significance of the ESPD framework, some limitations remain that are left for future investigations.

3.3.1 Theoretical Completeness

The theoretical framework established in Section 2.2 remains an area for deeper exploration. While the numerical designs presented in Section 2.4 are sufficient for guiding physical implementation, a complete theoretical study of the dynamic system in Eq.(8) remains of fundamental academic interest. Future work should focus on rigorously deducing the exact convergence conditions, calculating the precise steady-state point, and identifying the minimum initial performance criteria required. Given the inherent mathematical difficulty of such a non-linear and time-variant system, these specialized studies are reserved for the future.

3.3.2 Practical Cost and Optimization

Although the parallelized nature of the ESPD's detection stages theoretically preserves detection efficiency, the requirement for multiple detection events introduces a practical cost and operational burden, even without increasing the fundamental technological barriers. An L -level ESPD, with n auxiliary signals per level, requires a total of $(n + 1)^L$ base detections. While effective performance is typically achieved with only a few levels, this inherent multiplicative complexity increases the practical

cost, which may limit immediate commercial scalability. As shown in Section 2.4, the optimal choice of n and k is crucial as it dictates the convergence speed and the resulting DE-DCR trade-off. Enlarging k reduces DCR exponentially, while improving DE requires a lower k and larger n , and enlarging n increases detection cost. Therefore, designing the ESPD with optimal parameters constitutes a significant multi-objective optimization problem for the future.

This optimization problem also encompasses the optimal circuit design. To mitigate error propagation, minimizing the maximal circuit length is essential. Optimal designs could involve leveraging a binary-tree structure and defining the positive report event via a global, rather than the current level-by-level local, decision criterion, which expands the tree structure used in Section 2.1 with a local decision criterion. However, both problems require further and specific discussions: the general binary-tree structure results in non-independent distributions that are difficult to analyze, while the global decision criterion design must account for both device requirements and implementation convenience.

3.3.3 Physical Integrations and Experiments

Despite the convincing demonstration of effectiveness via numerical simulations in Section 2.4, the physical implementation of the ESPD scheme requires dedicated experimental validation. Furthermore, the seamless integration of controlled gates into various quantum optical tasks has not yet been fully investigated. Thus, both the physical realization of the ESPD scheme and its application to a wide range of tasks are key directions for future work. Reassuringly, as established in Section 3.1, no fundamental technological barriers prevent its current achievement.

4 Conclusion

In this paper, we have introduced the Enhanced Single-Photon Detector (ESPD) framework, a robust methodology for transforming low-performance, conventional SPDs into devices with performance comparable to or exceeding state-of-the-art superconducting SPDs. The ESPD scheme is characterized by significantly reduced technology requirements and immediate physical realizability using current quantum components. Our numerical analysis demonstrates that a legacy non-superconducting SPD, with $DE \approx 59\%$ and $DCR \approx 10^{-2}$, can be enhanced to one achieving $DE > 95\%$ and $DCR < 10^{-9}$. This dramatic boost circumvents the need for cryogenic superconducting materials, enabling the deployment of high-performance detection capabilities outside specialized laboratories. Furthermore, this enhancement allows the minimal tolerable channel transmission rate in quantum communication to be reduced by multiple orders of magnitude. The ESPD framework thus paves a clear, scalable path toward the commercialization and widespread implementation of high-performance quantum optical tasks.

Declarations

The author declares no financial or non-financial competing interests.

Author Contributions

Hao Shu (the unique author): study design, investigation, experiment, analysis, manuscript preparation.

Data and Code Availability

All data/codes generated or used during this study are included in this published article or can be found at <https://github.com/Hao-B-Shu/ESPD>.

References

- [1] Knill, E., Laflamme, R., Milburn, G.A.: scheme for efficient quantum computation with linear optics. *Nature* **409**, 46–52 (2001) <https://doi.org/10.1038/35051009>
- [2] Ding, X., Guo, Y.P., Xu, M.C., Liu, R.Z., Zou, G.Y., Zhao, J.Y., Ge, Z.X., Zhang, Q.H., Liu, H.L., Wang, L.J., Chen, M.C., Wang, H., He, Y.M., Huo, Y.H., Lu, C.Y., Pan, J.W.: High-efficiency single-photon source above the loss-tolerant threshold for efficient linear optical quantum computing. *Nature Photonics* **19**, 387–391 (2025) <https://doi.org/10.1038/s41566-025-01639-8>
- [3] Silva, M., Rötteler, M., Zalka, C.: Thresholds for linear optics quantum computing with photon loss at the detectors. *Physical Review A* **72**, 032307 (2005) <https://doi.org/10.1103/PhysRevA.72.032307>
- [4] Gisin, N., Gisin, B.: A local hidden variable model of quantum correlation exploiting the detection loophole. *Physics Letters A* **260**(5), 323–327 (1999) [https://doi.org/10.1016/S0375-9601\(99\)00519-8](https://doi.org/10.1016/S0375-9601(99)00519-8)
- [5] Márton, I., Bene, E., Vértesi, T.: Bounding the detection efficiency threshold in bell tests using multiple copies of the maximally entangled two-qubit state carried by a single pair of particles. *Physical Review A* **107**, 022205 (2023) <https://doi.org/10.1103/PhysRevA.107.022205>
- [6] Quintino, M.T., Araújo, M., Cavalcanti, D., Santos, M.F., Cunha, M.T.: Maximal violations and efficiency requirements for bell tests with photodetection and homodyne measurements. *Journal of Physics A: Mathematical and Theoretical* **45** (2012) <https://doi.org/10.1088/1751-8113/45/21/215308>
- [7] Vértesi, T., Pironio, S., Brunner, N.: Closing the detection loophole in bell experiments using qudits. *Physical Review Letters* **104**, 060401 (2010) <https://doi.org/10.1103/PhysRevLett.104.060401>
- [8] Rowe, M.A., Kielpinski, D., Meyer, V., Sackett, C.A., Itano, W.M., Monroe, C., Wineland, D.J.: Experimental violation of a bell’s inequality with efficient detection. *Nature* **409**, 791–794 (2001) <https://doi.org/10.1038/35057215>

- [9] Ma, W.C.: Efficiency bounds for testing a multiparticle bell inequality in an asymmetric configuration. *Physical Review A* **108**, 052216 (2023) <https://doi.org/10.1103/PhysRevA.108.052216>
- [10] Wittmann, B., Ramelow, S., Steinlechner, F., Langford, N.K., Brunner, N., Wiseman, H.M., Ursin, R., Zeilinger, A.: Loophole-free einstein–podolsky–rosen experiment via quantum steering. *New Journal of Physics* **14**, 053030 (2012) <https://doi.org/10.1088/1367-2630/14/5/053030>
- [11] Eberhard, P.H.: Background level and counter efficiencies required for a loophole-free einstein-podolsky-rosen experiment. *Physical Review A* **47**, 747–750 (1993) <https://doi.org/10.1103/PhysRevA.47.R747>
- [12] Clauser, J.F., Horne, M.A.: Experimental consequences of objective local theories. *Physical Review D* **10**, 526–535 (1974) <https://doi.org/10.1103/PhysRevD.10.526>
- [13] Ramelow, S., Mech, A., Giustina, M., Gröblacher, S., Wiecek, W., Beyer, J., Lita, A., Calkins, B., Gerrits, T., Nam, S.W., Zeilinger, A., Ursin, R.: Highly efficient heralding of entangled single photons. *Optics Express* **21**(6), 6707–6717 (2013) <https://doi.org/10.1364/OE.21.006707>
- [14] Ngah, L.A., Alibart, O., Labonté, L., D’Auria, V., Tanzilli, S.: Ultra-fast heralded single photon source based on telecom technology. *Laser & Photonics Reviews* **9** (2015) <https://doi.org/10.1002/lpor.201400404>
- [15] Davis, S.I., Mueller, A., Valivarthi, R., Lauk, N., Narvaez, L., Korzh, B., Beyer, A.D., Cerri, O., Colangelo, M., Berggren, K.K., Shaw, M.D., Xie, S., Sinclair, N., Spiropulu, M.: Improved heralded single-photon source with a photon-number-resolving superconducting nanowire detector. *Physical Review Applied* **18**, 064007 (2022) <https://doi.org/10.1103/PhysRevApplied.18.064007>
- [16] Stasi, L., Caspar, P., Brydges, T., Zbinden, H., Bussières, F., Thew, R.: High-efficiency photon-number-resolving detector for improving heralded single-photon sources. *Quantum Science and Technology* **8**(4), 045006 (2023) <https://doi.org/10.1088/2058-9565/ace54b>
- [17] Bennett, C.H., Brassard, G.: Quantum cryptography: Public key distribution and coin tossing. In: In Proceedings of IEEE International Conference on Computers (1984). <https://doi.org/10.1016/j.tcs.2014.05.025> . <https://www.sciencedirect.com/science/article/pii/S0304397514004241>
- [18] Lucamarini, M., Yuan, Z.L., Dynes, J.F., Shields, A.J.: Overcoming the rate–distance limit of quantum key distribution without quantum repeaters. *Nature* **557**(7705), 400–403 (2018) <https://doi.org/10.1038/s41586-018-0066-6>
- [19] Wang, S., He, D.Y., Yin, Z.Q., Lu, F.Y., Cui, C.H., Chen, W., Zhou, Z., Guo,

- G.C., Han, Z.F.: Beating the fundamental rate-distance limit in a proof-of-principle quantum key distribution system. *Physical Review X* **9**, 021046 (2019) <https://doi.org/10.1103/PhysRevX.9.021046>
- [20] Zeng, P., Zhou, H.Y., Wu, W.J., Ma, X.F.: Mode-pairing quantum key distribution. *Nature Communications* **13**, 3903 (2022) <https://doi.org/10.1038/s41467-022-31534-7>
- [21] Kanamori, H., Yokota, H., Tanaka, G., Watanabe, M., Ishiguro, Y., Yoshida, I., Kakii, T., Itoh, S., Asano, Y., Tanaka, S.: Transmission characteristics and reliability of pure-silica-core single-mode fibers. *Journal of Lightwave Technology* **4**(8), 1144–1150 (1986) <https://doi.org/10.1109/JLT.1986.1074837>
- [22] Nagayama, K., Kakui, M., Matsui, M., Saitoh, T., Chigusa, Y.: Ultra-low-loss (0.1484 db/km) pure silica core fibre and extension of transmission distance. *Electronics Letters* **38**, 1168–1169 (2002) <https://doi.org/10.1049/el:20020824>
- [23] Hirano, M., Haruna, T., Tamura, Y., Kawano, T., Ohnuki, S., Yamamoto, Y., Koyano, Y., Sasaki, T.: Record low loss, record high fom optical fiber with manufacturable process. In: *Optical Fiber Communication Conference/National Fiber Optic Engineers Conference 2013* (2013). <https://doi.org/10.1364/NFOEC.2013.PDP5A.7>. <https://opg.optica.org/abstract.cfm?URI=NFOEC-2013-PDP5A.7>
- [24] Tamura, Y., Sakuma, H., Morita, K., Suzuki, M., Yamamoto, Y., Shimada, K., Honma, Y., Sohma, K., Fujii, T., Hasegawa, T.: Lowest-ever 0.1419-db/km loss optical fiber. In: *2017 Optical Fiber Communications Conference and Exhibition (OFC)*, pp. 1–3 (2017)
- [25] Gottesman, D., Lo, H.K., Lütkenhaus, N., Preskill, J.: Security of quantum key distribution with imperfect devices. *Quantum Information and Computation* **4**, 325–360 (2004) <https://doi.org/10.26421/QIC4.5-1>
- [26] Shu, H.: Solve single photon detector problems. *Quantum* **7**, 1187 (2023) <https://doi.org/10.22331/q-2023-11-21-1187>
- [27] Shu, H.: Empty-Signal Detection: Proof-of-Principle Scheme for Arbitrarily Long-Distance Quantum Communication (2025). <https://arxiv.org/abs/2509.15884>
- [28] Albota, M.A., Wong, F.N.C.: Efficient single-photon counting at 1.55 μm by means of frequency upconversion. *Optics Letters* **29**(13), 1449–1451 (2004) <https://doi.org/10.1364/OL.29.001449>
- [29] Jiang, W.H., Liu, J.H., Liu, Y., Jin, G., Zhang, J., Pan, J.W.: 1.25ghz sine wave gating ingaas/inp single-photon detector with a monolithically integrated readout circuit. *Optics Letters* **42**(24), 5090–5093 (2017) <https://doi.org/10.1364/OL.42.005090>

- [30] Hu, P., Li, H., You, L.X., Wang, H.Q., Xiao, Y., Huang, J., Yang, X.Y., Zhang, W.J., Wang, Z., Xie, X.M.: Detecting single infrared photons toward optimal system detection efficiency. *Optics Express* **28**(24), 36884–36891 (2020) <https://doi.org/10.1364/OE.410025>
- [31] Chang, J., Los, J.W.N., Tenorio-Pearl, J.O., Noordzij, N., Gourgues, R., Guardiani, A., Zichi, J.R., Pereira, S.F., Urbach, H.P., Zwiller, V., Dorenbos, S.N., Esmail Zadeh, I.: Detecting telecom single photons with 99.5-2.07+0.5% system detection efficiency and high time resolution. *APL Photonics* **6**(3), 036114 (2021) <https://doi.org/10.1063/5.0039772>
- [32] Xu, G.Z., Zhang, W.J., You, L.X., Xiong, J.M., Sun, X.Q., Huang, H., Ou, X., Pan, Y.M., Lv, C.L., Li, H., Wang, Z., Xie, X.M.: Superconducting microstrip single-photon detector with system detection efficiency over 90% at 1550nm. *Photonics Research* **9**(6), 958–967 (2021) <https://doi.org/10.1364/PRJ.419514>
- [33] Craiciu, I., Korzh, B., Beyer, A.D., Mueller, A., Allmaras, J.P., Narváez, L., Spiropulu, M., Bumble, B., Lehner, T., Wollman, E.E., Shaw, M.D.: High-speed detection of 1550nm single photons with superconducting nanowire detectors. *Optica* **10**(2), 183–190 (2023) <https://doi.org/10.1364/OPTICA.478960>
- [34] Chen, J.P., Zhang, C., Liu, Y., Jiang, C., Zhang, W.J., Hu, X.L., Guan, J.Y., Yu, Z.W., Xu, H., Lin, J., Li, M.J., Chen, H., Li, H., You, L.X., Wang, Z., Wang, X.B., Zhang, Q., Pan, J.W.: Sending-or-not-sending with independent lasers: Secure twin-field quantum key distribution over 509 km. *Physical Review Letters* **124**, 070501 (2020) <https://doi.org/10.1103/PhysRevLett.124.070501>
- [35] Zhou, L., Lin, J.P., Xie, Y.M., Lu, Y.S., Jing, Y.M., Yin, H.L., Yuan, Z.L.: Experimental quantum communication overcomes the rate-loss limit without global phase tracking. *Physical Review Letters* **130**, 250801 (2023) <https://doi.org/10.1103/PhysRevLett.130.250801>
- [36] Liu, Y., Zhang, W.J., Jiang, C., Chen, J.P., Zhang, C., Pan, W.X., Ma, D., Dong, H., Xiong, J.M., Zhang, C.J., Li, H., Wang, R.C., Wu, J., Chen, T.Y., You, L.X., Wang, X.B., Zhang, Q., Pan, J.W.: Experimental twin-field quantum key distribution over 1000 km fiber distance. *Physical Review Letters* **130**, 210801 (2023) <https://doi.org/10.1103/PhysRevLett.130.210801>
- [37] Charaev, I., Batson, E.K., Cherednichenko, S., Reidy, K., Drakinskiy, V., Yu, Y., Lara-Avila, S., Thomsen, J.D., Colangelo, M., Incalza, F., Ilin, K., Schilling, A., Berggren, K.K.: Single-photon detection using large-scale high-temperature mgb2 sensors at 20 k. *Nature Communications* **15**, 3973 (2024) <https://doi.org/10.1038/s41467-024-47353-x>
- [38] Stolz, T., Hegels, H., Winter, M., Röhr, B., Hsiao, Y.F., Husel, L., Rempe, G., Dürr, S.: Quantum-logic gate between two optical photons with an average efficiency above 40%. *Physical Review X* **12**, 021035 (2022)

<https://doi.org/10.1103/PhysRevX.12.021035>

- [39] Shi, S.A., Xu, B., Zhang, K., Ye, G.S., Xiang, D.S., Liu, Y.B., Wang, J.Z., Su, D.Q., Li, L.: High-fidelity photonic quantum logic gate based on near-optimal rydberg single-photon source. *Nature Communications* **13**, 4454 (2022) <https://doi.org/10.1038/s41467-022-32083-9>
- [40] Pegoraro, F., Held, P., Lammers, J., Brecht, B., Silberhorn, C.: Realization of a c-not gate in a fully reconfigurable time-multiplexed photonic circuit. In: *Optica Quantum 2.0 Conference and Exhibition* (2025). <https://doi.org/10.1364/QUANTUM.2025.QM2A.4>. <https://opg.optica.org/abstract.cfm?URI=QUANTUM-2025-QM2A.4>
- [41] Harty, T.P., Allcock, D.T.C., Ballance, C.J., Guidoni, L., Janacek, H.A., Linke, N.M., Stacey, D.N., Lucas, D.M.: High-fidelity preparation, gates, memory, and readout of a trapped-ion quantum bit. *Physical Review Letters* **113**(22) (2014) <https://doi.org/10.1103/physrevlett.113.220501>
- [42] team, P.: A manufacturable platform for photonic quantum computing. *Nature* **641**(876–883) (2025) <https://doi.org/10.1038/s41586-025-08820-7>
- [43] Melchiorri, M., Daldosso, N., Sbrana, F., Pavesi, L., Pucker, G., Kompochohis, C., Bellutti, P., Lui, A.: Propagation losses of silicon nitride waveguides in the near-infrared range. *Applied Physics Letters* **86**(12) (2005)
- [44] Gruhler, N., Benz, C., Jang, H., Ahn, J.H., Danneau, R., Pernice, W.H.P.: High-quality si₃n₄ circuits as a platform for graphene-based nanophotonic devices. *Optics Express* **21**(25), 31678–31689 (2013)
- [45] Poot, M., Schuck, C., Ma, X.S., Guo, X., Tang, H.X.: Design and characterization of integrated components for silicon photonic quantum circuits. *Optics Express* **24**(7), 6843–6860 (2016) <https://doi.org/10.1364/OE.24.006843>
- [46] Chanana, A., Larocque, H., Moreira, R., Carolan, J., Guha, B., Melo, E.G., Anant, V., Song, J.D., Englund, D., Blumenthal, D.J., Srinivasan, K., Davanco, M.: Ultra-low loss quantum photonic circuits integrated with single quantum emitters. *Nature Communications* **13**, 7693 (2022) <https://doi.org/10.1038/s41467-022-35332-z>
- [47] Feng, L.T., Zhang, M., Xiong, X., Liu, D., Cheng, Y.J., Jing, F.M., Qi, X.Z., Chen, Y., He, D.Y., Guo, G.P., Guo, G.C., Dai, D.X., Ren, X.F.: Transverse mode-encoded quantum gate on a silicon photonic chip. *Physical Review Letters* **128**(6) (2022) <https://doi.org/10.1103/physrevlett.128.060501>
- [48] Yang, X., Sun, C.Y., Charlet, G., Tornatore, M., Pointurier, Y.: Digital-twin-based active input refinement for insertion loss estimation and qot optimization in c and c + l networks. *Journal of Optical Communications and Networking*

16(12), 1261–1274 (2024) <https://doi.org/10.1364/JOCN.537734>

- [49] Feng, L.T., Zhang, M., Liu, D., Cheng, Y.J., Song, X.Y., Ding, Y.Y., Dai, D.X., Guo, G.P., Guo, G.C., Ren, X.F.: Chip-to-chip quantum photonic controlled-not gate teleportation. *Physical Review Letters* **135**, 020802 (2025) <https://doi.org/10.1103/d53g-v8q6>